Volume 7 | Number 10 | 14 March 2019 | Pages 1513–1796

Journal of Materials Chemistry B

Materials for biology and medicine

rsc.li/materials-b

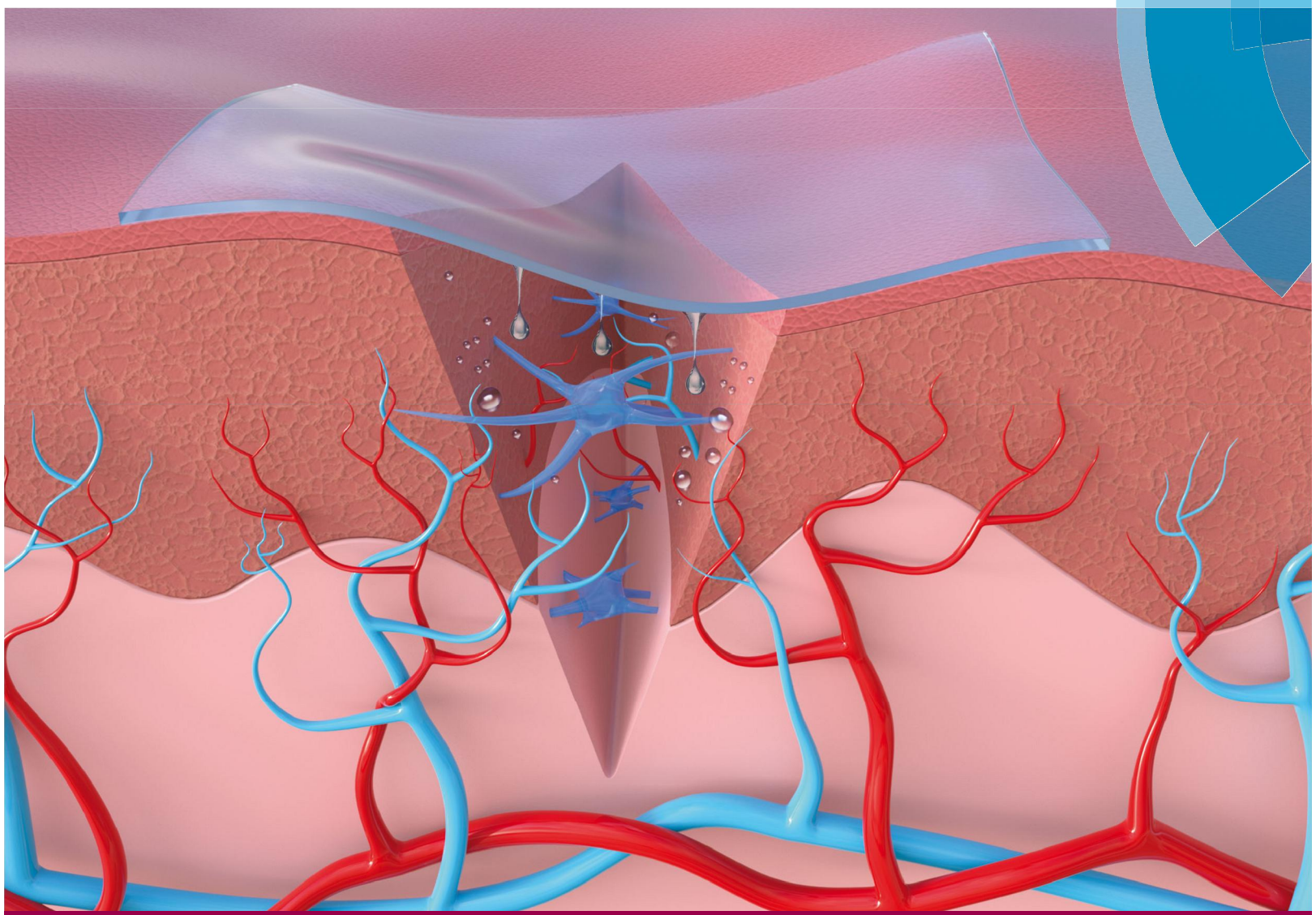

Themed issue: Hydrogel Properties and Applications

ISSN 2050-750X

ROYAL SOCIETY OF CHEMISTRY | Celebrating IYPT 2019

PAPER

Jie Zheng, Jian Xiao, Jiang Wu *et al.*

Zwitterionic poly(sulfobetaine methacrylate) hydrogels with optimal mechanical properties for improving wound healing *in vivo*

Journal of Materials Chemistry B

PAPER

Cite this: J. Mater. Chem. B, 2019, 7, 1697

Zwitterionic poly(sulfobetaine methacrylate) hydrogels with optimal mechanical properties for improving wound healing *in vivo*†

Huacheng He, ‡[a] Zecong Xiao,‡[b] Yajiao Zhou,[b] Anqi Chen,[b] Xuan Xuan,[b] Yanyan Li,[b] Xin Guo,[b] Jie Zheng, *[c] Jian Xiao*[b] and Jiang Wu*[b]

Zwitterionic hydrogels, as highly hydrated and soft materials, have been considered as promising materials for wound dressing, due to their unique antifouling and mechanical properties. While the viscoelasticity and softness of zwitterionic hydrogels are hypothetically essential for creating adaptive cellular niches, the underlying mechanically regulated wound healing mechanism still remains elusive. To test this hypothesis, we fabricated zwitterionic poly(sulfobetaine methacrylate) (polySBMA) hydrogels with different elastic moduli prepared at different crosslinker contents, and then applied the hydrogels to full-thickness cutaneous wounds in mice. *In vivo* wound healing studies compared the mechanical cue-induced effects of soft and stiff polySBMA hydrogels on wound closure rates, granulation tissue formation and collagen deposition. Collective results showed that the softer and more viscoelastic hydrogels facilitated cell proliferation, granulation formation, collagen aggregation, and chondrogenic ECM deposition. Such high wound healing efficiency by the softer hydrogels is likely attributed to stress dissipation by expanding the cell proliferation, the up-regulation of blood vessel formation, and the enhanced polarization of M2/M1 macrophages, both of which would provide more oxygen and nutrients for cell proliferation and migration, leading to enhanced wound repair. This work not only reveals a mechanical property–wound healing relationship of zwitterionic polySBMA hydrogels, but also provides a promising candidate and strategy for the next-generation of wound dressings.

Received 1st October 2018,
Accepted 21st January 2019

DOI: 10.1039/c8tb02590h

rsc.li/materials-b

1. Introduction

Wound dressing is a key approach to address a grand challenge of wound healing for different traumatic, thermal, acute, and chronic wounds affecting millions of people globally.[1] Generally speaking, wound healing is a very sophisticated process that requires different tissues and cells to cooperate and communicate in a way to realize cell proliferation and tissue remodeling (*e.g.* fibroblast migration, endothelial cell angiogenesis, and epithelial cell re-epithelization) after hemostasis and inflammation.[2] Despite different wound types (*e.g.*, traumatic, acute, chronic, exuding, and dry wounds), the design of nontoxic/nonallergenic wound dressings usually should satisfy several combinatory factors: protection of wounds from bacterial infection, high adsorption ability, improved cell proliferation, enhanced anti-inflammation, desirable humidity environment, and/or ease of removal and replacement without pain.[3,4]

Among different wound dressing materials, hydrogels are considered as the most promising wet-and-soft materials for wound dressing because of their high water content, and adequate mechanical/elastic, stimuli-responsive, and some self-recovery/self-healing properties,[5–8] allowing them to well mimic wound soft tissues. Most of the soft tissues (*e.g.* skin, blood vessels and nerves) not only possess high mechanical toughness and extensibility, but also exhibit strain-induced viscoelastic behavior.[9] However, conventional hydrogels suffer from weak mechanical properties and poor mechanical responses to different external stimuli,[10] which greatly limits their uses as wound soft tissue substitutes. Extensive studies have reported that the biomechanics of hydrogels and other soft materials (*e.g.* topographical and intrinsic structure, and mechanical toughness/strength/modulus/elasticity) is critical not only for serving as supporting substrates to retain tissue integrity and cell activity,[11] but also for the transversion of biophysical cues to biochemical responses that regulate cell behaviors for tissue regeneration.[12] These cross-talks between biophysical and biochemical stimuli initiates cell proliferation,

[a] College of Chemistry and Materials Engineering, Wenzhou University, Wenzhou, Zhejiang 325027, P. R. China. E-mail: woody870402@hotmail.com
[b] School of Pharmaceutical Sciences, Wenzhou Medical University, Wenzhou, Zhejiang 325035, P. R. China. E-mail: xfxj2000@126.com
[c] Department of Chemical and Biomolecular Engineering, The University of Akron, Akron, OH, 44325, USA. E-mail: zhengj@uakron.edu

† Electronic supplementary information (ESI) available. See DOI: 10.1039/c8tb02590h

‡ The authors contributed equally to this work.

migration, differentiation, and remodeling during the wound healing process.[13,14] Specifically, chemical (*e.g.* polymer components, crosslinkers) and mechanical (*e.g.* toughness, stiffness, modulus) properties of hydrogels (not limited to wound dressings) generally have influence on cell behaviors and wound repair effect.[15] For instance, hydrogels with optimal mechanical properties can better stimulate keratinocytes proliferation/migration, angiogenesis and neovascularization, and bFGF and TGF-β1 secretion, and enhance blood vessel formation, re-epithelialization, extracellular matrix synthesis and remodeling, thus promoting wound closure.[16,17] Hydrogels with too low or too high stiffness will compromise the wound repair effect. These studies indicate that the presence of wound dressings allows cells to respond to micromechanical stimuli at wound sites. On the other hand, cells can also rapidly produce extracellular matrix that will exert forces back to wound dressing materials.[18,19] Apart from a chronic wound healing model, many previous studies have also shown that mechanical properties of hydrogels could be used and tuned to control and stimulate cell differentiation.[20,21]

These hydrogel dressing examples have shown that the biomechanics of biomaterials are pivotal for the fate, toxicity, and function of cells and tissues during the wound healing process. However, there is a dearth of systematic research to better elucidate the poorly understood problem of how proteins and cells respond and adapt to hydrogel-based wound dressings. An in-depth study of this problem will provide mechanistic insights into the interactions between wound dressings and tissues at the hydrogel–wound interface, and thus promote the development of a new generation of wound dressings with long-term healing efficiency.[22]

Significant research efforts have been made to develop poly(ethylene glycol) PEG-based polymers for wound healing; however, less attention is paid to zwitterionic materials, some of which have demonstrated their super low-fouling property *in vitro* and anti-inflammatory property *in vivo*. Zwitterionic polymers are among the most popular antifouling materials, because zwitterionic polymers can be more hydrophilic than PEG to strongly attract a layer of water molecules for resisting unwanted protein adsorption that will further lead to inflammation at wounds.[23] Herein, we prepared zwitterionic sulfated poly(sulfobetaine methacrylate) (polySBMA) hydrogels and applied them to full-thickness excisional acute wound regeneration in mice, with a particular attention to wound healing efficiency in response to mechanical softness/stiffness of polySBMA hydrogels with elastic modulus ranging from a softness of 10 kPa to a hardness of 60 kPa. Collective results showed that the softer polySBMA hydrogels could speed up wound healing efficiently through the intrinsic elastic impulse to improve neovascularization. Thus, zwitterionic hydrogels exhibit great potential as promising wound dressings.

2. Materials and methods

2.1. Materials

[2-(Methacryloyloxy)ethyl]dimethyl-(3-sulfopropyl)ammonium hydroxide (SBMA, M_n = 279.35) as a monomer, poly(ethylene glycol)dimethacrylate (PEGDMA, M_n = 550) as a crosslinker, and photoinitiator Irgacure 2959 (I2959), as an initiator, were all purchased from Sigma-Aldrich. Hematoxylin–eosin (HE) and Masson's Trichrome Stain Kit were purchased from Sigma-Aldrich, St. Louis, MO. Phosphate buffer saline (PBS) was purchased from Sigma-Aldrich. Horseradish peroxidase (HRP)-conjugated goat anti-human lgG (H + L) was purchased from Beijing Biosynthesis Biotechnology Co. Human umbilical vein endothelial cell (HUVEC) was purchased from the Cell Storage Center of Wuhan University (Wuhan, China). Other cell culture reagents were purchased from Invitrogen (Carlsbad, CA). Deionized water was used as received.

2.2. Preparation of polySBMA hydrogels with different elastic moduli

Different polySBMA hydrogels were prepared using a previous method.[24] Here, the elastic modulus of polySBMA hydrogels was achieved by the chemical crosslinker percentage. The monomer (SBMA) was firstly dissolved in de-ionized (DI) water. The cross linker (PEGDMA) was varied from 0.1%, 0.5%, 1% to 5% (*versus* monomer w/w), and the initiator (I2959) (final 1% *versus* monomer w/w) was added and completely dissolved in the above solutions at room temperature. The final concentration of the monomer was 4 M. Then, the solution mixture was transferred onto a pair of glass plates separated by poly(tetrafluoroethylene) (PTFE) (with a thickness of 3 mm or 1 mm). Next, the photo-polymerization reaction was carried out at room temperature with 362 nm UV light SB-100P (Spectroline) for 30 mins. After the polymerization, the hydrogels were removed from the plates and immersed in a large volume of DI water (1 L), which was changed every 3 h for 5 days to ensure that non-reacted initiators or monomers were totally removed from the hydrogels.

2.3. Determination of equilibrium water content (EWC) of the hydrogels

The hydrated hydrogels were used to quantify their EWC by their mass difference between the hydrated state and fully dried state. The weight of the hydrogels in the swollen state was recorded as W_s, and that of the lyophilized hydrogels was recorded as W_d. The EWC was determined by the weight change of hydrogels in the swollen state and dry state using the following eqn (1):

$$\mathrm{EWC}\,(\%) = \frac{(W_s - W_d)}{W_s} \times 100\% \qquad (1)$$

The swelling kinetics of the polySBMA hydrogels was tested using a gravimetric method. Prepared swollen hydrogels of the same size were first freeze-dried (W_d) and then immersed in deionized water. At each time interval, the samples were wiped with filter paper to remove the water. The weight of the hydrogels was measured as W_t. The degree of swelling ratio was calculated using the following eqn (2):

$$\text{Swelling ratio}\,(\%) = \frac{W_t - W_d}{W_d} \times 100\% \qquad (2)$$

The mass loss rate of the hydrogels was estimated by weighing the hydrogels everyday recorded as W_e and the initial water

content of the swollen hydrogels was recorded as W_i. Then, the water retaining capacity was obtained using the following eqn (3):

$$\text{Water retaining content } (\%) = \frac{W_i - W_c}{W_i} \times 100\% \quad (3)$$

2.4. Morphology of polySBMA hydrogels

The morphology of the hydrogels was examined by scanning electron microscopy (SEM) (Hitachi S-3000 SEM). Swollen polySBMA hydrogel samples were firstly frozen in liquid nitrogen and then lyophilized for at least 24 h. Before the SEM examination, the cross sectional part of the dried hydrogels was coated with gold by ion sputtering. SEM analysis was carried out with an acceleration voltage of 10 keV and a probe current of 25 mA.

2.5. Compressive mechanical tests of hydrogels

The swollen hydrogels immersed in water for more than 5 days with a cylindrical shape (8 mm in diameter and 3 mm in thickness) were placed on the compression plate. Five disks of each hydrogel were compressed to failure at a compressive strain rate of 1 mm min^{-1} using an Instron 3343 (Instron Co, USA) with a 10 N load cell at room temperature. The modulus was calculated from the linear portion of the stress–strain curve.

2.6. Protein adsorption measurements

Nonspecific protein adsorption to the hydrogels was determined by quantifying HRP-conjugated anti-IgG adsorption using tissue culture polystyrene (TCPS) as a control. The samples were firstly incubated with 1 μg ml^{-1} anti-IgG for 1.5 h and rinsed with PBS six times. The TCPS and the hydrogels were then removed and placed in 24-well plates separately. Then, 1 ml *o*-phenylenediamine (OPD 1 μg ml^{-1}) in 0.1 M citrate phosphate buffer (pH 5.0) containing 0.03% hydrogen peroxide was added. Next, this enzyme–substrate activity reaction was stopped by adding an equal volume of H_2SO_4 (2 M) after 15 min. Finally, the relative protein adsorption percentage compared to TCPS was measured by the appearance of tangerine color at 492 nm.

2.7. *In vitro* HUVEC cell surface attachment assay

TCPS and polySBMA hydrogels were placed individually in 24-well plates. After being irradiated for 30 min under UV light, 10^5 cells per ml HUVEC cells were seeded onto the samples in RPMI 1640 medium. After the cells were grown for 24 h at 37 °C, 5% CO_2 and 100% humidity, the samples were photographed using a 4× Nikon Eclipse TE2000U microscope.

2.8. *In vivo* wound healing model and analysis

The animal models were performed using the same procedure as our previous paper.[25] 6 to 7 week-old male C57BL/6 mice with a weight of 25 g were purchased from the Animal Center of Chinese Academy of Sciences, Shanghai, China. All animal experiments were performed in accordance with the National Institutes of Health Guide Concerning the Care and Use of Laboratory Animals and the guidelines approved by the Animal Experimentation Ethics Committee of Wenzhou Medical University, Wenzhou, China. Mice were maintained on a standard diet for at least 7 d before the experiment, and water was provided *ad libitum*. The temperature (23–25 °C), humidity (35–60%), and photoperiod (12 h light/dark cycle) were kept constant. Firstly, the mice were anaesthetized with an intraperitoneal injection of 4% chloral hydrate (0.1 ml/10 g), and the dorsal area was shaved. 0.5-mm-thick donut-shaped silicone splints (external diameter of 16 mm, internal diameter of 8 mm) were fixed on either side of the dorsal midline using 6-0 Prolene sutures. Two full-thickness cutaneous wounds were made using a 6 mm round skin biopsy punch (Acuderm® inc., Ft Lauderdale, FL, USA) on each side of the dorsal midline. Secondly, the wound sites were measured using a digital camera to determine the original wound area. The wounds were then treated with our sample hydrogels. Each sample was used in 7 animals with 14 wounds per group. All hydrogel dressings were cut into 7 mm diameter dishes using a punch immediately before applying to the wounds. Then, the hydrogel dressings were covered with Tegaderm™ transparent dressing (3 M Health Care, Germany) to prevent infection and wrapped in a thin layer of self-adhesive bandages to deter chewing of the splints. At days 0, 7, 10, 14, and 17 post-treatment, the wound closure rate was determined by measuring the wound area using Image-Pro Plus to trace the wound margin (wound closure rate% = (wound area_{day0} − wound $\text{area}_{day\#}$)/wound area_{day0} × 100%). At day 7 or 20 post-surgery, C57BL/6 mice were anesthetized with 4% chloral hydrate and sacrificed by cervical dislocation. The wound sites were excised, and the tissues were processed for histological evaluation.

2.9. Histological analysis

For histological analysis, the skin was fixed in 4% paraformaldehyde in 0.01 M phosphate buffered saline (PBS, pH = 7.4) overnight, dehydrated in graded ethanol series and then embedded in paraffin. The tissue was sectioned into 5 μm thick slices for hematoxylin and eosin (H&E) (Beyotime Institute of Biotechnology, China) staining and for observation of collagen formation by Masson's trichrome staining (Beyotime), using standard reported procedures.[26] Sections were analyzed and images were captured using a Nikon ECLIPSE 80i microscope (Nikon, Japan).

2.10. Immunofluorescent staining

CD-31 (ab28364, Abcam), Ki67 (ab15580, Abcam), CD 163 (ab182422, Abcam) and CD 68 (ab955, Abcam) were observed using their respective antibodies following our previous paper.[23] The skin tissue sections, prepared by a microtome with 5 μm thickness, were deparaffinized, rehydrated, and then immersed in 3% H_2O_2 and 80% carbinol for 15 min at room temperature to block the endogenous peroxidase activity. The tissue sections were heated for antigen recovery in 10 mM sodium citrate buffer (pH 6.0), and after washing, the samples were blocked using 5% bovine serum albumin (BSA) (Beyotime) for 30 min at room temperature. Skin sections (on 7 day post wound) were stained with rabbit polyclonal anti-CD31 (1 : 200), anti-Ki67 (1 : 200), rabbit polyclonal anti-CD 163 (1 : 200) and mouse monoclonal anti-CD 68 (1 : 100) diluted in phosphate-buffered saline

(PBS) containing 1% bovine serum albumin (BSA) overnight at 4 °C. Fluorescence secondary antibodies IgG Alexa Fluor® 488 and goat anti-mouse IgG Alexa Fluor® 647 (ab150083, 1 : 1500, Abcam) were diluted with phosphate-buffered saline (PBS), respectively, and then incubated at 37 °C for 60 min. After DAPI-stained nuclear for 5 min and coverslipping with anti-fluorescent quencher, the fluorescent images were taken by a Nikon confocal laser microscope (Nikon, A1 PLUS, Tokyo, Japan).

2.11. Statistical analysis

All the data were expressed as means ± standard deviations (SD). The statistical data were compared using the unpaired Student's *t*-test. Significant difference was considered if the two-tailed *P*-values were <0.05. For all tests, $^{*}P < 0.05$, $^{**}P < 0.01$ and $^{***}P < 0.001$.

3. Results and discussion

3.1. Physicochemical properties of the polySBMA hydrogels

To fabricate the hydrogels with controllable mechanical properties, here we used different crosslinking percentages (0.1%, 0.5%, 1%, and 5%) to tune the polySBMA hydrogels from soft to stiff. Fig. 1A shows the typical compressive strain–stress curves of the polySBMA hydrogels. As the crosslinker content increased from 0.1% to 5%, the polySBMA hydrogels significantly and monotonically increased their compressive stress from 0.015 MPa to 0.35 MPa (Fig. 1A) and elastic modulus from 6.7 kPa to 50.4 kPa (Fig. 1B) at a compressive strain of 80% without failure. For the convenience of system notation, based on the compressive mechanical properties of the polySBMA hydrogels, the polySBMA hydrogels with a low elastic modulus of <12 kPa prepared at 0.1% and 0.5% crosslinker contents are defined as soft-1 and soft-2 hydrogels, while the remaining two hydrogels with a high elastic modulus of >48 kPa prepared at 1% and 5% crosslinker contents are defined as stiff-1 and stiff-2 hydrogels. Fig. 1C shows that, on the one hand, the four polySBMA hydrogels were highly hydrated with a consistently high EWC of $>80\%$, demonstrating the hydrophilic nature of the polySBMA hydrogels. On the other hand, the increase of crosslinker content also slightly reduced the EWC by 10% simply because of the more compact and tightly interpenetrating network. Similarly, Fig. 1D shows the swelling kinetics of the four hydrogels in PBS solution. It can be seen that all hydrogels swell rapidly to achieve equilibrium swelling within ~4 h. Consistently, the increase of the crosslinkers reduced hydrogel swelling; accordingly, the swell ratios were 1392.2% for soft-1 (0.1%), 965.0% for soft-2 (0.5%), 542.8% for

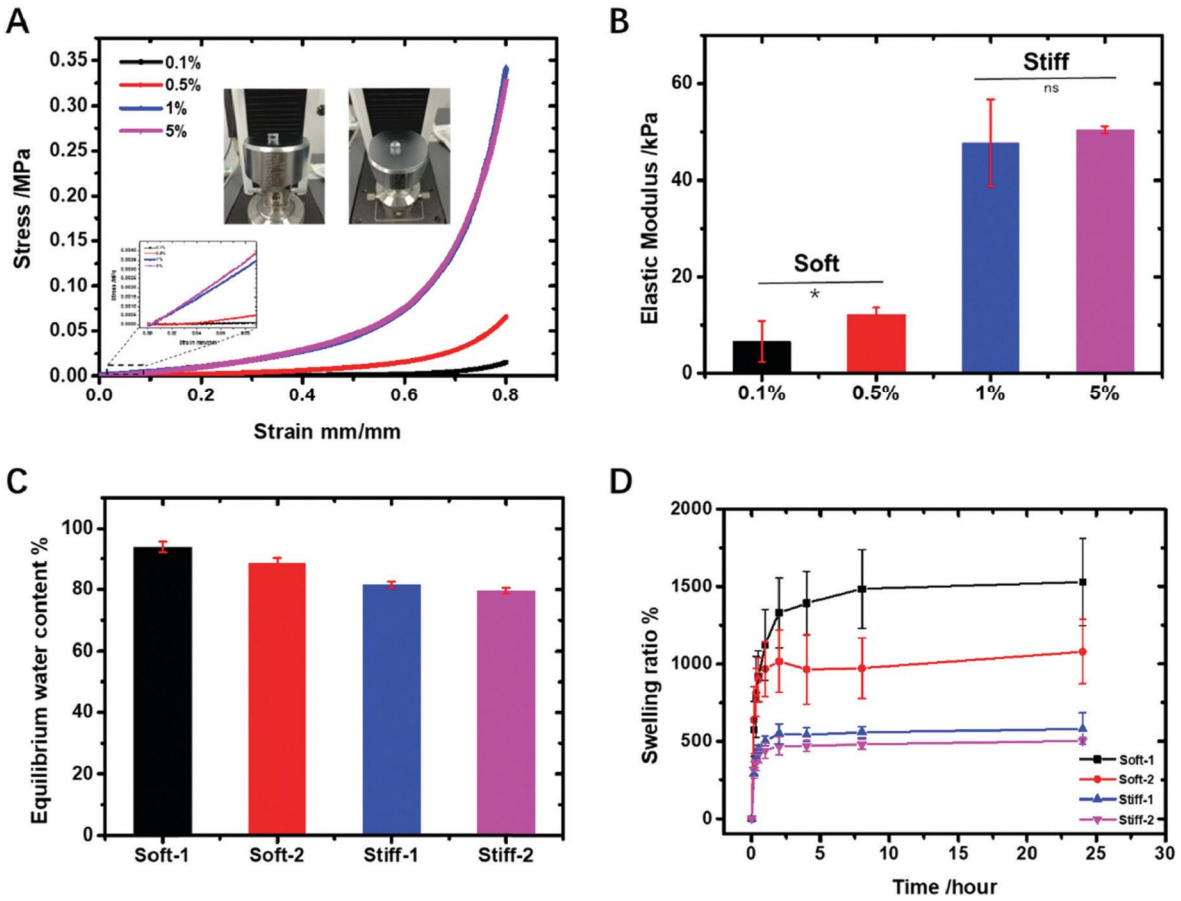

Fig. 1 Compressive properties of zwitterionic polySBMA hydrogels prepared by different cross-linking densities from 0.1% to 5%. (A) Compressive stress–strain curves, (B) elastic modulus, (C) equilibrium water content (EWC), and (D) swelling kinetics of as-prepared polySBMA hydrogels.

stiff-1 (1%), and 469.0% for stiff-1 (5%), respectively. This phenomenon became even more pronounced for the soft-1 hydrogels, which swelled almost 3 times higher than the stiff hydrogels. Thus, the introduction of crosslinkers greatly suppresses the expansion of gel networks. As expected, the swollen transparent hydrogels become mechanically weak, due to the breaking of hydrogen bonds and lower polymer volume fraction.

Fig. 2A shows the optical properties of the four polySBMA hydrogels at the as-prepared state. Except for the stiff-2 hydrogel (5% of crosslinkers) showing semitransparent optical properties, the other three hydrogels exhibited optical transparency. SEM images in Fig. 2B showed the internal morphology of the four polySBMA hydrogels. It can be clearly seen that each individual hydrogel possessed a relatively uniform pore structure, but the pore size distribution decreased from 20 μm to 5 μm with the increase in crosslinkers. The highly porous structures in all hydrogels resemble natural macromolecular cellar matrix systems, suitable for cell proliferation and migration, as well as oxygen permeation, especially for chronic wounds as wound dressing improves neovascularization. Fig. 2C shows that due to the strong ionic solvation of zwitterionic polymers, all the polySBMA hydrogels retain a high water content of ~70% at room temperature for 7 days. Such high water retention property of soft-1, soft-2, stiff-1 and stiff-2 hydrogels is advantageous for keeping the wound sites moist.

3.2. *In vitro* antifouling properties of polySBMA hydrogels

Antifouling properties of polySBMA polymers are critical for wound healing.[23] Our previous work has demonstrated that polySBMA polymer brushes could achieve an ultralow fouling level of protein adsorption (<0.3 ng cm^{-2}) and also excellent hydrophilicity, salt resistance, and biocompatibility.[27–29] Different from previous work focusing on the antifouling property of polySBMA brushes, here we examined the protein adsorption on polySBMA hydrogels using enzyme-linked immunosorbent assay (ELISA), where tissue culture polystyrene (TCPS) was used as a control to set a complete monolayer protein adsorption (100%). As shown in Fig. 3A, as compared to TCPS, all the polySBMA hydrogels significantly reduce the adsorbed protein amounts to 5–20%. Stiffer polySBMA hydrogels exhibited slightly better protein resistance than softer hydrogels, probably because higher elastic moduli and the more compact porous structures prevent protein adsorption on and adaption to the hydrogel surface.[24] Further data analysis results showed that under the consideration of error bars, there was no significant difference (ns) between the soft (0.1% and 0.5%) and stiff (1% and 5%) hydrogels. To further test the ability of polySBMA hydrogel to resist cell attachment, a cell assay was carried out to probe the additional antifouling property of the hydrogels. GFP-expressed HUVEC cells were used to co-culture with polySBMA hydrogels at 37 °C for 24 h. After culturing, hydrogels were gently washed with PBS to remove any unbound or weakly bound cells. Finally, the images of the four hydrogels were taken under a fluorescent microscope with the same excitation light and exposure time. As shown in Fig. 3B, in sharp contrast to TCPS whose surface was covered by an almost full layer of cells, all polySBMA hydrogels exhibited negligible cell attachment. Even though the polySBMA hydrogels had been soaked in

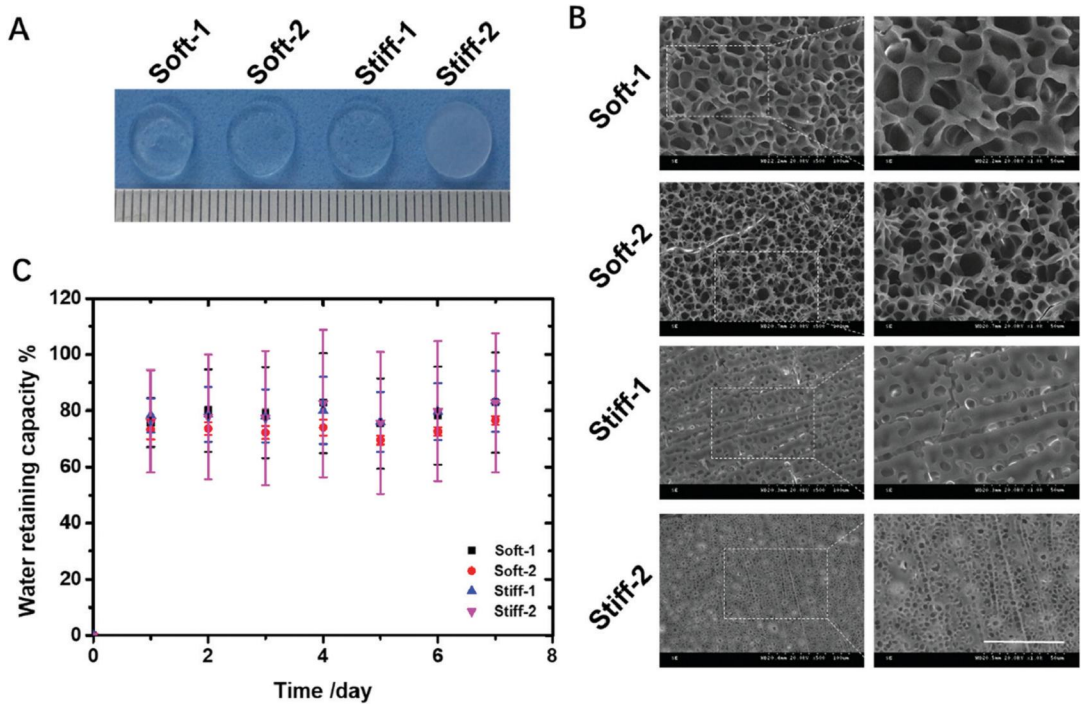

Fig. 2 Physical properties of zwitterionic polySBMA hydrogels prepared at different cross-linking densities from 0.1% to 5% (namely soft-1, soft-2, stiff-1, and stiff-2 hydrogels). (A) Visual inspection of appearance, (B) SEM images (scale bar = 50 μm), and (C) water retaining capacity of the four polySBMA hydrogels.

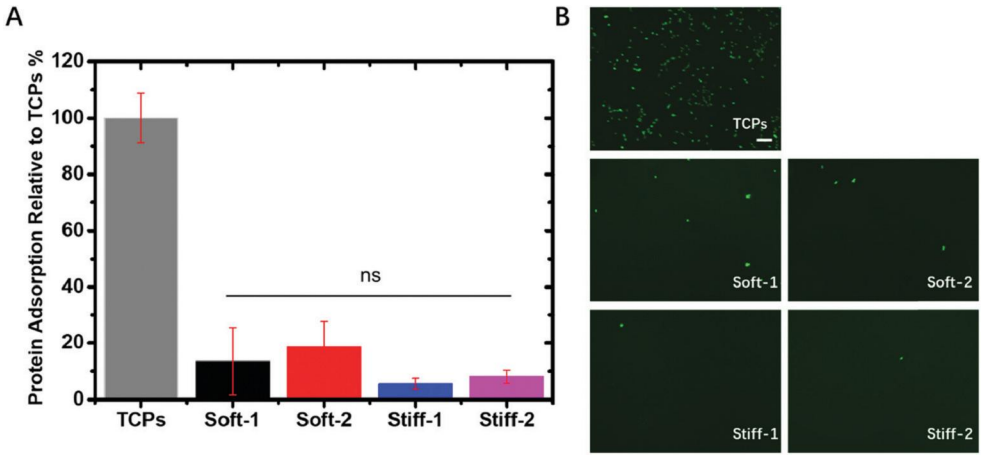

Fig. 3 Antifouling properties of zwitterionic polySBMA hydrogels prepared at different cross-linking densities from 0.1% to 5%. (A) IgG protein adsorption and (B) cell adhesion (scale bar = 500 μm) on all the polySBMA hydrogels relative to TCPS.

serum-containing medium for two weeks, the polySBMA hydrogels, regardless of their mechanical softness or stiffness, were able to keep their non-fouling property and did not allow cell adhesion on their surfaces, demonstrating the intrinsic nature of the antifouling property.

3.3. *In vivo* wound regeneration properties of polySBMA hydrogels

After polySBMA hydrogels demonstrated their excellent antifouling properties to resist both protein adsorption and cell adhesion *in vitro*, here we applied the polySBMA hydrogels to full-thickness cutaneous wounds in C57BL/6 mice, and then examined their wound healing efficiency as a function of elastic modulus. At first glance, both the visual images of wound bed closure (Fig. 4A) and the corresponding mimetic trace of wound bed closure (Fig. 4B) were used to assess the *in vivo* wound-healing efficacy of the polySBMA hydrogels at different time points during 20 days treatment. Compared to the control group treated with PBS, all the polySBMA hydrogel-treated groups showed enhanced wound regeneration behavior and no obvious sign of inflammation or infection near the wound area. It appears that the growth of new epidermis extended to

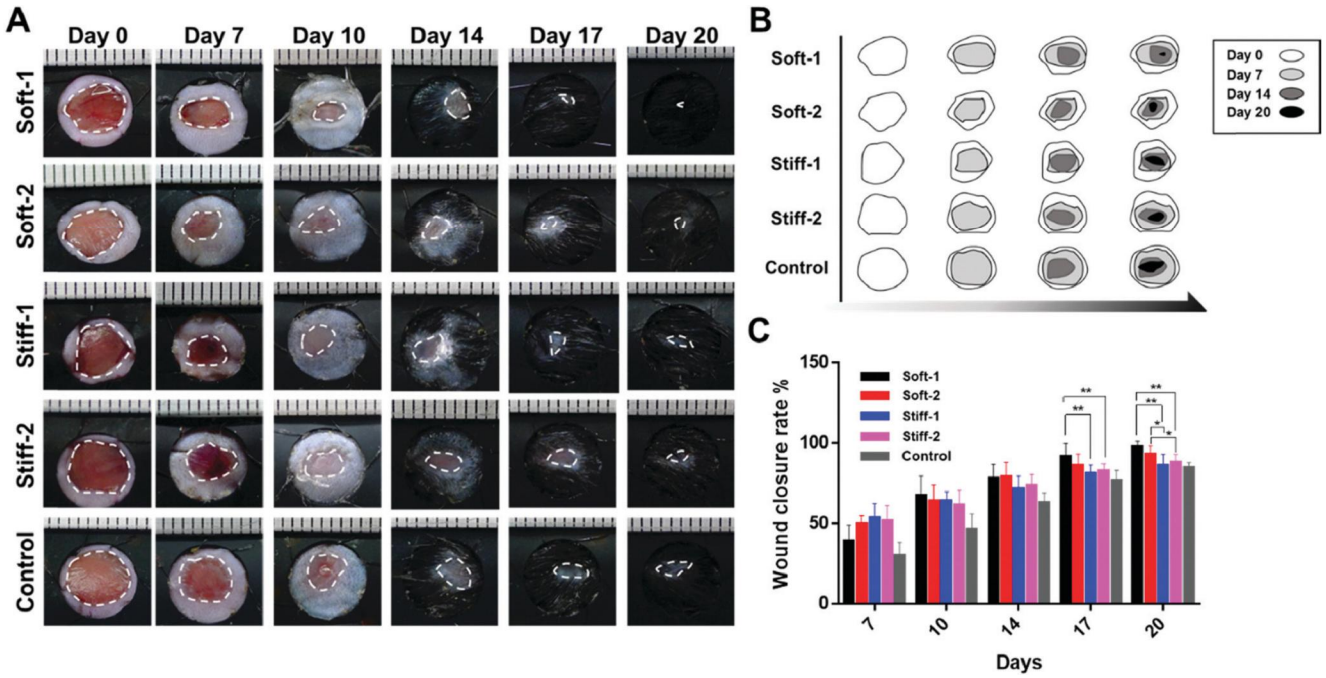

Fig. 4 *In vitro* wound healing efficacy of zwitterionic polySBMA hydrogels prepared at different cross-linking densities. (A) Photographs of excised wounds, (B) schematic of wound closure trace, and (c) quantitative evaluation of wound closure rates for all hydrogel- and saline (control)-treated wounds on days 0, 7, 10, 14, 17 and 20 in each group. Error bars indicate SD. Significant differences between sample means are indicated: $^{**}P < 0.01$, $^{*}P < 0.05$ where $n > 6$.

the center of all hydrogel treated wounds, resulting in a reduction in wounded area. Among the four polySBMA hydrogel treated groups, the wounds treated with soft-1 and soft-2 hydrogels regenerated faster than those treated with the stiff-1 and stiff-2 hydrogels. Specifically, after 20 days treatment, the soft-1 and soft-2 polySBMA hydrogels enabled the wounds to completely heal with almost no scars, while siff-1 and stiff-2 treated wounds still exhibited obvious residual wound area. Quantitatively, Fig. 4C analyzed the restoration area ratio of the wound bed. Consistent with visual inspection, soft-1 and soft-2 hydrogels showed significantly higher wound closure rates than the stiff-1 and stiff-2 hydrogels at every time point. The final wound closure rates of the soft hydrogels were 98.1% and 93.2%, as compared to those of the stiff-1 (87.5%), stiff-2 (89.5%), and control (85.0%) hydrogels. The ~10% enhancement in wound regeneration of the soft polySBMA hydrogels could be attributed to soft mechanical properties, high water content, and nanomorphological structures, all of which are more compatible with soft skin, thus providing a "suturing" effect at the wound site to enhance wound contraction and closure during the early stage of the wound-healing process. As shown in Fig. 4C, on day 20, there were significant differences between the soft-2 and stiff-1 gels and between the soft-2 and stiff-2 gels, in which both p values were lower than 0.01 ("*" indicates $p < 0.05$). However, the results on day 17 did not show obvious improvements between soft-2 and stiff-1/stiff-2 gels. In general, both soft hydrogels showed significant enhancement of wound regeneration compared to both stiff hydrogels on day 17 and day 20. This result further confirms that the wound healing efficiency is sensitive to the mechanical properties of the hydrogels.

Considering that a typical wound healing process comprises granulation tissue formation, re-epithelialization, and collagen deposition, here we used the H&E staining of wounds treated with polySBMA hydrogels on day 7 and day 20 to evaluate the granulation and epidermal formation. As shown in Fig. 5A, H&E stained sections of the wounded skins treated with polySBMA hydrogels exhibited a markedly higher epidermis and granulation construction than those of the control group. Specifically, on day 7, the hydrogel-treated groups developed a full length of epidermal layer, while less re-epithelialization was observed in the control group. On day 20, the hydrogel-treated groups were able to connect tightly regenerated dermis and fill with appendants under a fully healed epithelialization layer, while the control group still had larger unhealed wound areas with a thin granulation construction. Similar to our earlier *in vivo* wound closure results, while the H&E staining for all the groups showed no pathological changes, the softer hydrogels had a smaller wound closure area and thicker granulation formation than the stiffer hydrogels. Furthermore, H&E staining was performed on the wound cross sections to identify and quantify the center of the wound (Fig. 5B). The results show that the mean length of the granulation gap at day 7/day 20 for wounds treated with soft-1, soft-2, stiff-1, stiff-2, and PBS was 3.0/1.2, 3.4/1.8, 3.8/2.5, 4.0/2.0 and 4.5/3.2 μm, respectively (Fig. 5C). The mean granulation tissue thickness was on average 1.6/1.6, 1.5/1.3, 1.4/1.2, 1.3/1.2, and 1.0/0.7 μm for wounds treated with soft-1, soft-2, stiff-1, stiff-2, and PBS at day 7/day 20, respectively (Fig. 5D). Altogether, these results suggest that the softer polySBMA hydrogels significantly accelerate skin wound healing *via* improved granulation tissue formation and epithelial tissue regeneration, relative to the stiffer hydrogels.

In the final remodeling stage of wound healing, a mass deposition of collagen (a predominant structural protein in skin) is necessary to reconstruct dermal tissue at wound sites effectively.

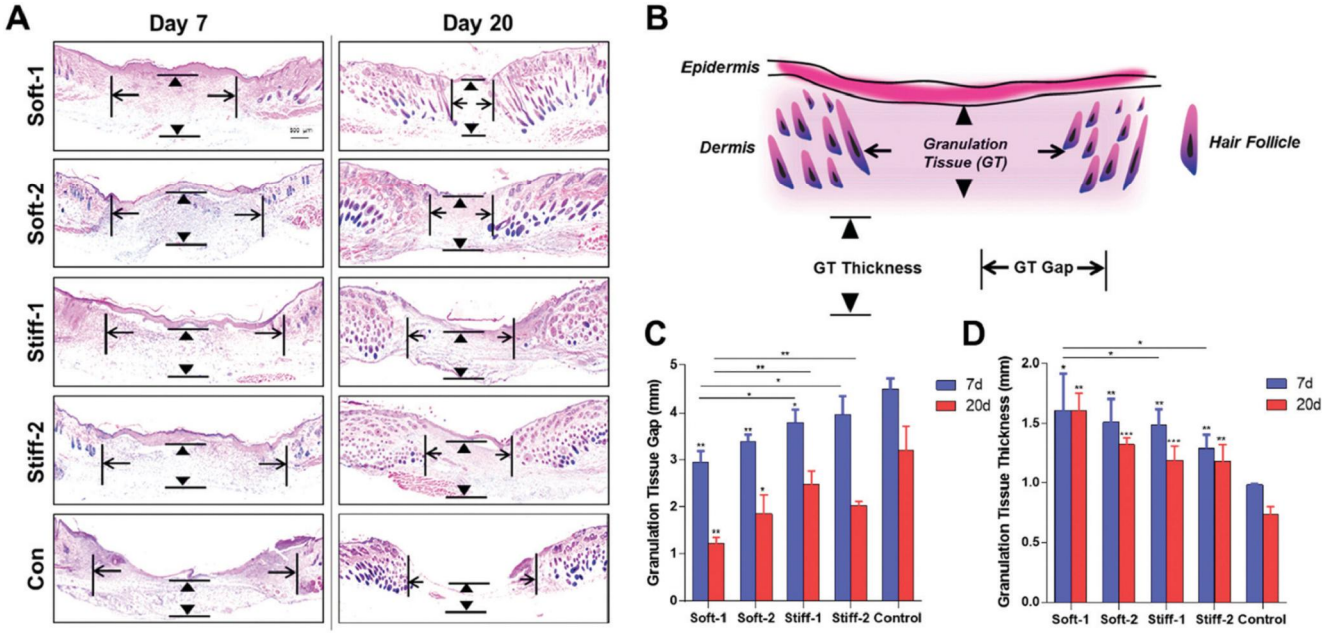

Fig. 5 H&E staining of wound sections obtained from the different zwitterionic polySBMA hydrogel-treated and control groups at day 7 and day 20 post-operation. (A) H&E stained images for skin wounds treated with polySBMA hydrogels and PBS on day 7 and day 20. (B) Schematic measurement of granulation tissue thickness and granulation gap.[30,31] (C) Quantification of granulation tissue gap and thickness on days 7 and 20. $^{**}P < 0.01$, $^{*}P < 0.05$, $n > 5$.

Masson's trichrome staining (MTS) on day 7 and day 20 was used to determine the histological collagen deposition (staining in blue). As shown in Fig. 6A, on day 7, all polySBMA-treated wounds were covered by a more intense blue color as compared to the control group, demonstrating that collagen deposition was most enhanced in hydrogel-treated wounds, leading to thicker wound granulation formation and a smaller wound gap. On day 20, the accelerated granulation tissue formation and collagen deposition became even more pronounced. Among the four hydrogel-treated wounds, it can be seen that the softer hydrogel-treated groups not only had extensive and thick collagen deposition both in the wound center and wound edge reflected by the deep blue staining, but also had the most orderly collagen arrangement compared with other groups at both 7 and 20 days. We also observed that the soft hydrogel-treated wounds had more densely packed collagen fibers with parallel arrangements as compared to the stiff hydrogel-treated wounds with loosely packed collagen fibers running in irregular arrangements, or the control with nothing. Quantitatively, Fig. 6B shows the statistical analysis of collagen deposition on day 20. Clearly, the mean collagen deposition density in PBS-, soft-1-, soft-2-, stiff-1-, and stiff-2-treated wounds was 4539.4 ± 1386.6, 42882.3 ± 15839.2, 15887.5 ± 6386.6, 11528.3 ± 1380.3, and 6091.7 ± 1526.0 mm^{-2}, respectively. So, the soft hydrogel-treated wounds represented 3–7 fold increase in collagen deposition, relative to the wounds treated with stiff hydrogels. These results further confirm the effectiveness of wound healing by wound remodeling *via* more collagen deposition. It is important to mention that collective data from Fig. 4 (wound closure rates and image), Fig. 5 (granulation formation), and Fig. 6 (collagen deposition) indicate that the wound in the control group on day 20 did not completely close, and the partial wound closure was likely due to the contraction effect in the wound. We should also note that severed muscle and deep staining with trypan do not necessarily indicate the existence of normal tissue; instead, they could also be an indicator of newly regenerated skin in our case.

3.4. Soft polySBMA hydrogels accelerate neovascularization more than stiff polySBMA hydrogels

Among the wound healing processes that could be triggered by GFs, neovascularization and angiogenesis are crucial to tissue engineering.[32] The formation of new vasculature is fundamental

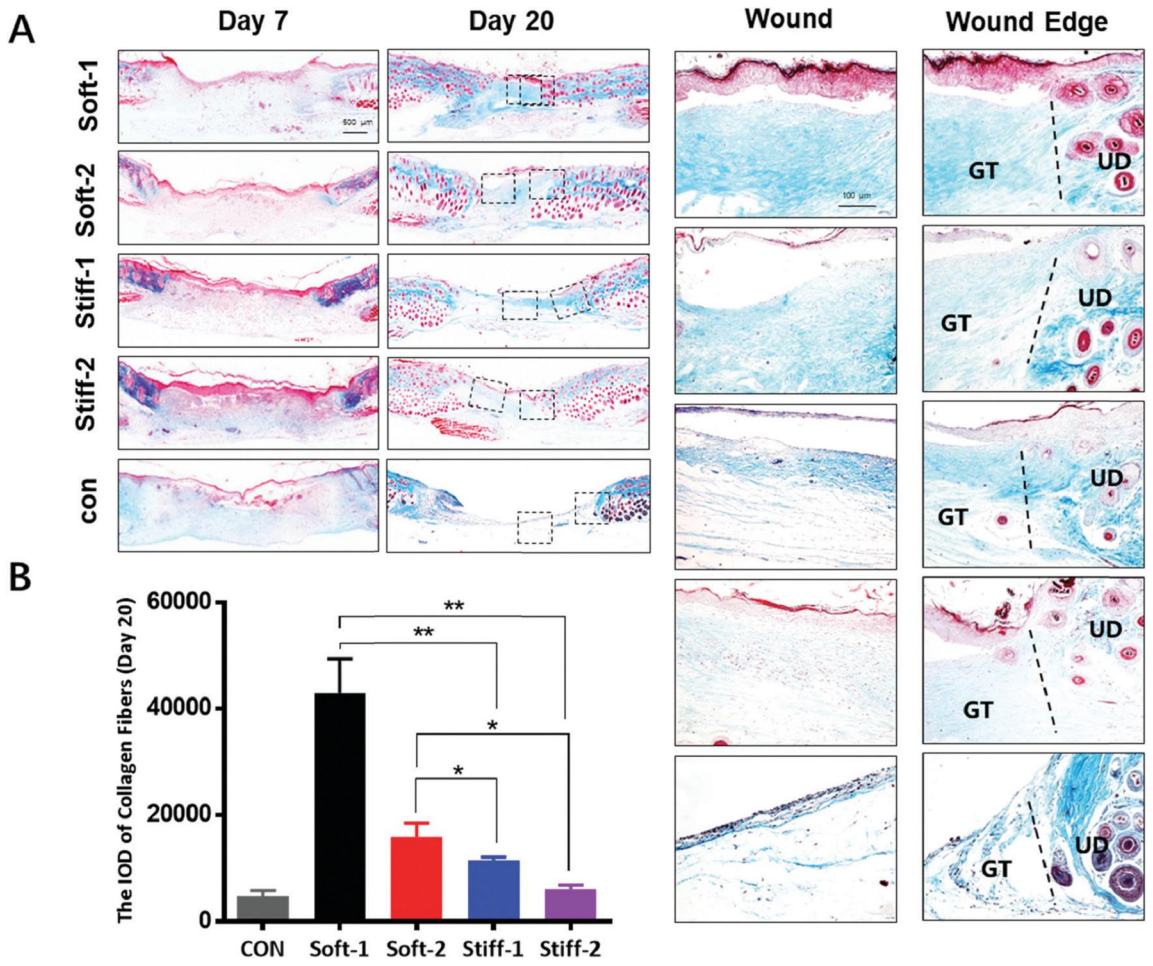

Fig. 6 Masson's trichrome staining (MTS) of wound sections obtained from the different zwitterionic polySBMA hydrogel-treated and control groups on day 7 and day 20 post-operation, showing collagen deposition and maturity. (A) MTS images of skin wounds treated with polySBMA hydrogels and PBS on day 7 and day 20 (scale bar = 500 μm), as well as close-up MTS images at the wound center and wound edge on day 20 (scale bar = 100 μm). (B) Quantification of collagen deposition density in the wound sites on day 20 by optical blue density (IOD), $^{**}P < 0.01$, $^{*}P < 0.05$, $n > 5$.

to powering the wound regeneration. To confirm the newly formed vessels found in the wound area, we also performed immunofluorescence staining of CD31 endothelial cell marker to identify the new blood vessel formation on day 7. As shown in Fig. 7A, wounds treated with both softer hydrogels exhibited a higher amount of CD31 cells than wounds treated with stiffer hydrogels. To further assess this outcome, the overall area covered by the CD31 cells in the hydrogel groups was quantified to determine their density in the wound area. Fig. 7B shows that the density of CD31 cells was 17.21%, 13.4%, 4.3%, and 1.7% for soft-1-, soft-2-, stiff-1-, and stiff-2-treated wounds, respectively, consistent with immunofluorescence staining images. Thus, softer hydrogel wound dressings will promote angiogenesis and neovascularization, which in turn provide more oxygen and nutrients to the wounds and guide the cells for wound remolding such as granulation and collagen formation (Fig. 7C). Thus, our results suggest that soft hydrogels accelerate wound healing *via* improved granulation tissue formation and epithelial tissue regeneration, possibly by increasing the collagen deposition and the formation of new blood vessels.

3.5. Soft polySBMA hydrogels enhance cell proliferation and M2/M1 macrophages more than stiff polySBMA hydrogels

In order to further understand the mechanical regulation of the wound healing mechanism, Ki-67 protein (also known as MKI67) was used as a cellular maker for evaluating cell proliferation during the wound repair process. As shown in Fig. 8A, soft-1 and soft-2 dressings up-regulated cell proliferation as compared to stiff-1 and stiff-2 dressings at early stages of wound healing on day 7, as evidenced by significant differences of $***p < 0.001$ between the soft-1 and two stiff hydrogels and of $**p < 0.01$ between the soft-2 and two stiff hydrogels, respectively (Fig. 8C). In addition, these cells could further secrete granulation matrix and different types of growth factors to promote wound regeneration. This enhanced cell proliferation once again confirms a beneficial role of soft polySBMA hydrogels in wound repair.

Macrophage activation of M2 (anti-inflammatory) *versus* M1 (pro-inflammatory) is considered as an important factor to promote angiogenesis and tissue remodeling. In our previous work, we have demonstrated that zwitterionic polySBMA hydrogels enable the polarization of macrophages from M1 to M2 through enhanced anti-inflammatory proteins to achieve wound healing functions.[33] Here, we also quantified M1 (stained by CD-68, red color) and M2 macrophages (stained by CD-163, green color) of the four hydrogels and compared them with the control group. It can be seen in Fig. 8B and D that the soft-1 and soft-2 dressings were much more active to up-regulate M2 macrophages at day 7 than the stiff-1 and stiff-2 dressings, as evidenced by the presence of more green color in Fig. 8B and a significant difference of $***p < 0.001$ between the soft hydrogels and stiff hydrogels in Fig. 8D. In line with the wound closure rate, granulation formation, and collagen deposition, the results of the expression of M2/M1 macrophages again confirm the positive role of soft hydrogels in wound regeneration.

We also conducted cell toxicity experiments, when co-cultured with polySBMA hydrogels, to verify their biocompatibility. As shown in Fig. S1-A (ESI†), as compared to

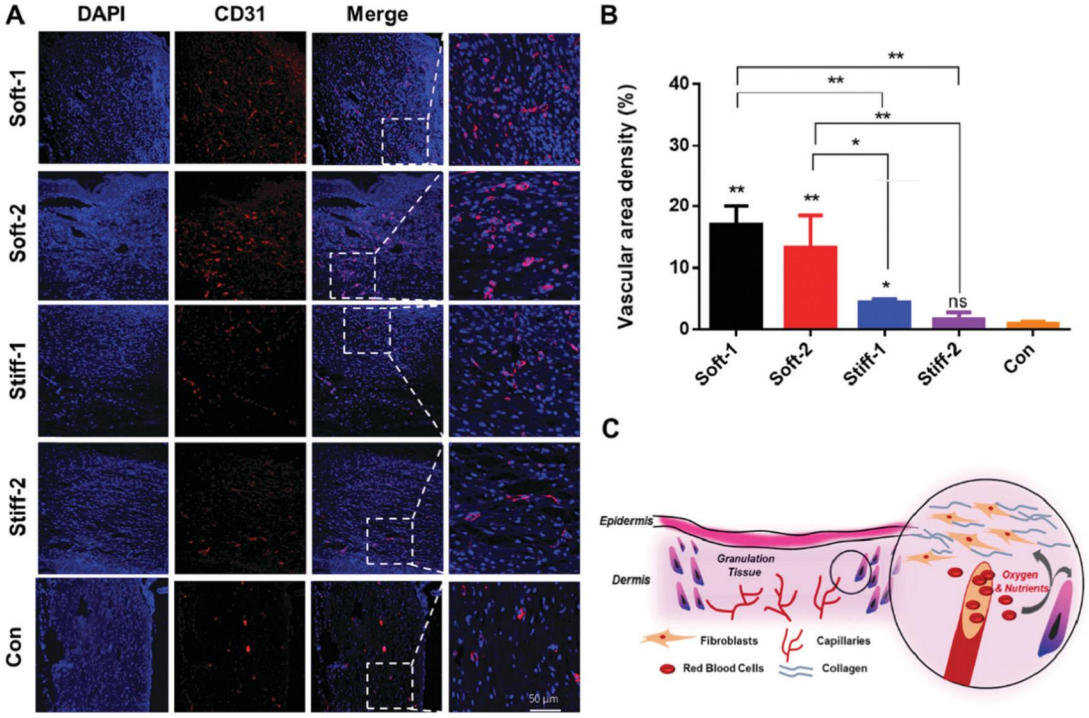

Fig. 7 CD31 staining for characterizing neovascularization in wound sites of the different zwitterionic polySBMA hydrogel-treated and control groups. (A) CD31 (red) and DAPI (blue) staining for new blood vessels on day 7 post-operation. (B) Quantitative analysis of newly formed blood vessels as measured by vascular area density on day 7. $**P < 0.01$, $*P < 0.05$, $n > 5$. (C) Schematic of neovascularization at wound sites.

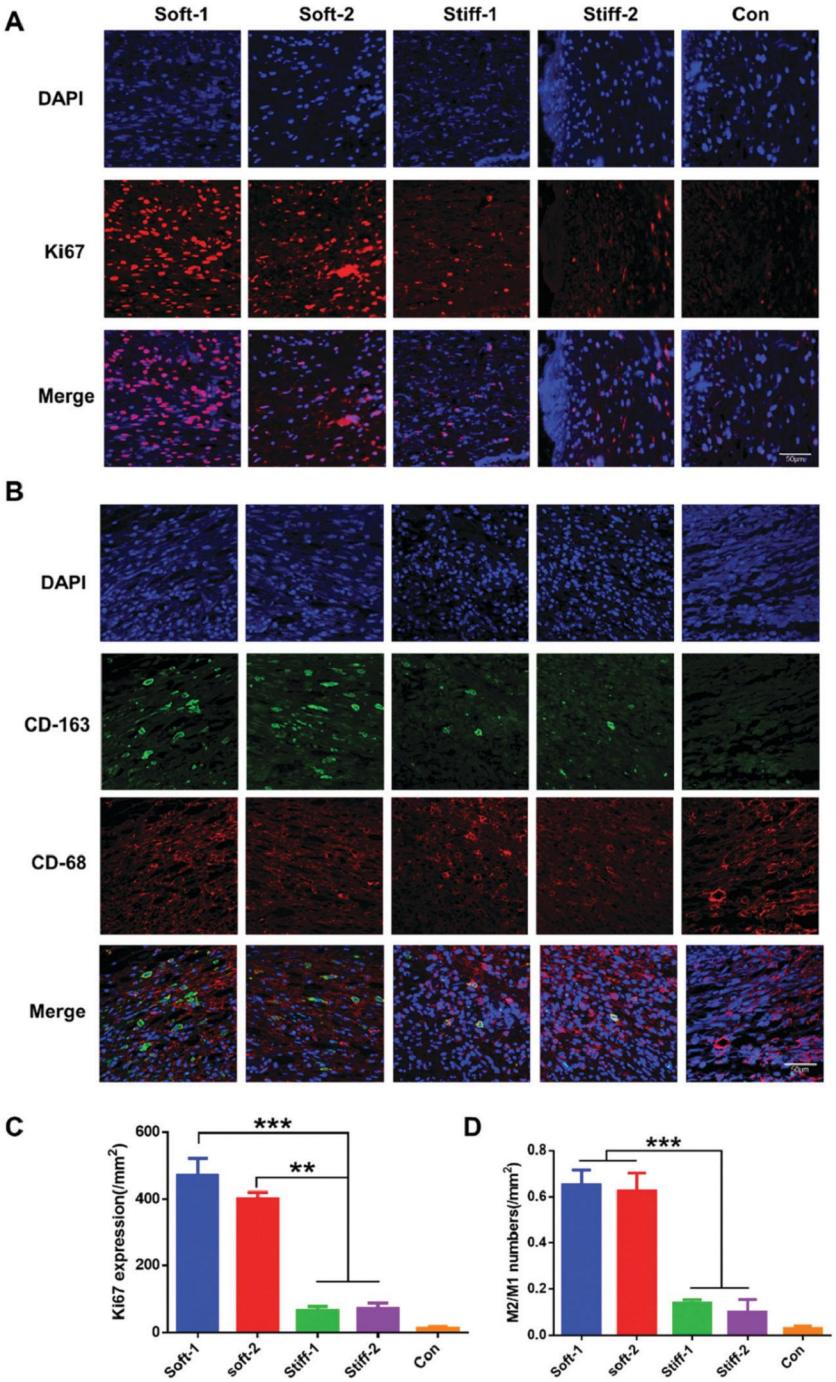

Fig. 8 (A) Immunofluorescent staining of wound sites on day 7 post-wounding for cell proliferation (Ki67, red) and DAPI-stained nuclei (blue). (B) Immunofluorescent staining of wound sites on day 7 post-wounding for M1 (CD-68, red), and M2 macrophage (CD-163, green) and DAPI-stained nuclei (blue). (C) Quantitative evaluation of Ki67 expression of the four hydrogel-treated groups and the control on day 7. (D) Quantitative evaluation of M2/M1 of the four hydrogel-treated groups and the control. Significant differences between samples are defined by $***P < 0.001$, $**P < 0.01$, where $n > 6$.

the control group, the four hydrogel-treated groups showed no obvious differences in terms of the morphology and proliferation of HaCat cells. Furthermore, the CCK-8 assay in Fig. S1-B (ESI†) showed that upon 24 h incubation, the cell viability for all the hydrogel groups and the control group displayed no obvious differences. Both the cell toxicity and viability results indicate the good biocompatibility of the polySBMA hydrogels.

4. Conclusion

In this study, zwitterionic polySBMA hydrogels with different mechanical properties were prepared and used as wound dressings to treat full-thickness dermal wounds in mice. First, all the polySBMA hydrogels demonstrated high water content and retention ability and super antifouling properties to prevent unwanted protein adsorption and cell adhesion *in vitro*. Then, the softer

polySBMA hydrogels exhibited better wound healing efficiency *in vivo* than the stiffer ones, through their enhanced wound closure, accelerated granulation tissue formation, increased collagen deposition, and improved new blood vessel formation. Finally, collective data revealed a correlation between the mechanical property and wound healing efficiency, demonstrating a simple and possibly generalizable approach to achieve better wound healing efficiency by simply controlling the mechanical properties of hydrogels as wound dressings.

Conflicts of interest

There are no conflicts to declare.

Acknowledgements

J. W. and H. H. are thankful for the financial support from the National Natural Science Funding of China (81601615 and 81701809), the Zhejiang Qianjiang Talent Project under the Grant QJD1803015 and Zhejiang Provincial Natural Science Foundation of China under Grant No. LGF19H180008. J. Z. is thankful for the financial support from NSF (DMR-1806138 and CMMI-1825122).

References

1 W. Loke, S. Lau, L. L. Yong, E. Khor and C. K. Sum, *J. Biomed. Mater. Res.*, 2000, **53**, 8–17.
2 P. S. Martin, *Science*, 1997, **276**, 75–81.
3 J. S. Boateng, K. H. Matthews, H. N. E. Stevens and G. M. Eccleston, *J. Pharm. Sci.*, 2008, **97**, 2892–2923.
4 Y. H. Kim, K. T. Hwang, J. T. Kim and S. W. Kim, *J. Wound Care*, 2015, **24**, 536–542.
5 M. D. Konieczynska, J. C. Villacamacho, C. Ghobril, M. Perezviloria, K. M. Tevis, W. A. Blessing, A. Nazarian, E. K. Rodriguez and M. W. Grinstaff, *Angew. Chem.*, 2016, **55**, 9984–9987.
6 N. Roy, N. Saha, T. Kitano and P. Saha, *Soft Mater.*, 2010, **8**, 130–148.
7 B. Mirani, E. Pagan, B. Currie, M. A. Siddiqui, R. Hosseinzadeh, P. Mostafalu, Y. S. Zhang, A. Ghahary and M. Akbari, *Adv. Healthcare Mater.*, 2017, **6**, 1700718.
8 S. Sakai, M. Tsumura, M. Inoue, Y. Koga, K. Fukano and M. Taya, *J. Mater. Chem. B*, 2013, **1**, 5067–5075.
9 T. S. Stashak, E. Farstvedt and A. Othic, *Clin. Tech. Equine Pract.*, 2004, **3**, 148–163.
10 S. A. Eming, P. Martin and M. Tomiccanic, *Sci. Transl. Med.*, 2014, **6**, 265sr6.
11 R. O. Hynes, *Science*, 2009, **326**, 1216–1219.
12 B. Cheng, M. Lin, G. Huang, Y. Li, B. Ji, G. M. Genin, V. Deshpande, T. J. Lu and F. Xu, *Phys. Life Rev.*, 2017, 88–119.
13 V. Llopishernandez, M. Cantini, C. Gonzalezgarcia, Z. A. Cheng, J. Yang, P. M. Tsimbouri, A. J. Garcia, M. J. Dalby and M. Salmeronsanchez, *Sci. Adv.*, 2016, **2**, e1600188.
14 J. Barthes, H. Ozcelik, M. Hindie, A. Ndreuhalili, A. Hasan and N. E. Vrana, *BioMed Res. Int.*, 2014, 921905.
15 P. Olczyk, Ł. Mencner and K. Komosinskavassev, *BioMed Res. Int.*, 2014, 747584.
16 G. Xia, Y. Liu, M. Tian, P. Gao, Z. Bao, X. Bai, X. Yu, X. Lang, S. Hu and X. Chen, *J. Mater. Chem. B*, 2017, **5**, 3172–3185.
17 S. Chen, J. Shi, X. Xu, J. Ding, W. Zhong, L. Zhang, M. Xing and L. Zhang, *Colloids Surf., B*, 2016, **140**, 574–582.
18 D. Y. Shu and F. J. Lovicu, *Prog. Retinal Eye Res.*, 2017, **60**, 44–65.
19 E. Hadjipanayi, V. Mudera and R. A. Brown, *J. Tissue Eng. Regener. Med.*, 2009, **3**, 77–84.
20 A. J. Engler, S. Sen, H. L. Sweeney and D. E. Discher, *Cell*, 2006, **126**, 677–689.
21 R. G. Wells and D. E. Discher, *Sci. Signaling*, 2008, **1**, pe13.
22 S. R. Peyton and A. J. Putnam, *J. Cell. Physiol.*, 2005, **204**, 198–209.
23 J. Wu, Z. Xiao, A. Chen, H. He, C. He, X. Shuai, X. Li, S. Chen, Y. Zhang and B. Ren, *Acta Biomater.*, 2018, **71**, 293–305.
24 H. He, X. Xuan, C. Zhang, Y. Song, S. Chen, X. Gong, B. Ren, J. Zheng and J. Wu, *Langmuir*, 2018, DOI: 10.1021/acs.langmuir.8b01755.
25 J. Wu, J. Zhu, C. He, Z. Xiao, J. Ye, Y. Li, A. Chen, H. Zhang, X. Li and L. Lin, *ACS Appl. Mater. Interfaces*, 2016, **8**, 18710–18721.
26 J. Wu, J. Ye, J. Zhu, Z. Xiao, C. He, H. Shi, Y. Wang, C. Lin, H. Zhang, Y. Zhao, X. Fu, H. Chen, X. Li, L. Li, J. Zheng and J. Xiao, *Biomacromolecules*, 2016, **17**, 2168–2177.
27 J. Wu, C. Zhao, W. Lin, R. Hu, Q. Wang, H. Chen, L. Li, S. Chen and J. Zheng, *J. Mater. Chem. B*, 2014, **2**, 2983–2992.
28 J. Wu, C. Zhao, R. Hu, W. Lin, Q. Wang, J. Zhao, S. M. Bilinovich, T. C. Leeper, L. Li and H. M. Cheung, *Acta Biomater.*, 2014, **10**, 751–760.
29 L. Li, S. Chen, J. Zheng, B. D. Ratner and S. Jiang, *J. Phys. Chem. B*, 2005, **109**, 2934–2941.
30 X. Zhao, H. Wu, B. Guo, R. Dong, Y. Qiu and P. X. Ma, *Biomaterials*, 2017, **122**, 34–47.
31 J. Devalliere, K. Dooley, Y. Hu, S. S. Kelangi, B. E. Uygun and M. L. Yarmush, *Biomaterials*, 2017, **141**, 149–160.
32 J. Li, Y. P. Zhang and R. S. Kirsner, *Microsc. Res. Tech.*, 2003, **60**, 107–114.
33 J. Wu, Z. Xiao, A. Chen, H. He, C. He, X. Shuai, X. Li, S. Chen, Y. Zhang and B. Ren, *Acta Biomater.*, 2018, **71**, 293–305.